314 KSME Journal, Vol. 10, No. 3, pp. 314~320, 1996

Analysis of the Machining Process of Sintered Bronze

Ki-Ju Kang and N. A. Fleck

(Received November 27, 1995)

The machining process observed during orthogonal cutting tests for sintered bronze of 11%, 23% and 33% porosity is analyzed. Each step of the machining process, that is, compaction due to the indentation by a cutting tool, the shear local to the tip of the tool and the fracture near the chip root are simulated by a mechanical model based on classical theories of indentation, machining and fracture. The presented models make it possible to predict the several behaviors of the machining, such as the types of chip formation, maximum cutting pressure and chip wave length. Good agreement between the experimental results and the predictions is found.

Key Words: Sintered Material, Indentation, Fracture Mechanics, Machining, Cutting Pressure, Chip Wave Length

1. Introduction

Recently sintered materials are widely used as machine parts and structural members. Sintered metals are useful for mass production of precision components of complex shape. Ultra hard and high tough machine tools and oil-less bearings are the typical examples. Engineering ceramics are also manufactured by sintering and their high hardness and heat-resistibility make them ones of most promising engineeing materials. As increasing use of the sintered materials, their machining becomes an important subject. Because of the porosity, it shows unique characteristics different from fully dense materials.

Authors have reported some test results of orthogonal machining for sintered bronze (Fleck et al., 1996). The dependence of the cutting mechanism and cutting force upon the initial porosity of the bronze, the depth of cut and the rake angle of the tool was investigated. It was shown that machining of the sintered bronze is composed of three processes, that is, compaction due to indentation by tool, shear local to tip of the tool, and fracture near the chip root. Relative dominance among the processes seems to determine types of chip formation, such as continuous or discontinuous chip.

In this papar, the each process of machining of the sintered bronze is mechanically analyzed. Several phenomena observed in the experiments are explained theoretically. The results are expected to be applicable to machining of any sintered or porous materials, for examples, ceramics, rocks and concretes.

2. Experimental Results

Spherical bronze powder of diameter $50\pm10\ \mu$m was pressureless sintered in a vacuum furnace for one hour. The final porosity, f was controlled at 33%, 23% and 11%, by setting the sintering temperature at 750℃, 800℃ and 850℃, respectively. Figure 1 shows the stress-strain curves. The mechanical properties are summarized in Table 1. Only for $f=33\%$, somewhat significant difference was observed between the compressive yield stress σ_{yc} and tensile yield stress σ_{yt} as 55MPa versus 34MPa. The fracture toughness K_c was measured using a 3-point bend rig: it was found that the values are typical for sintered bronzes.

The specimens were machined using a specially

* Dept. of Mechanical Engineering Chonnam National University, Kwangju 500-757, Republic of Korea

** Cambridge University Engineering Dept., Trumpington St., Cambridge, CB2 1PZ, England

Table 1 Mechanical properties of porous bronze specimens

Porosity, f	H_v	E (GPa)	σ_{yt} (MPa)	σ_{yc} (MPa)	K_c (MPa$\sqrt{m}$)
33%	22.7	19	34	55	1.5
23%	34.0		87	95	8.9
11%	62.9	80	142	140	16.5

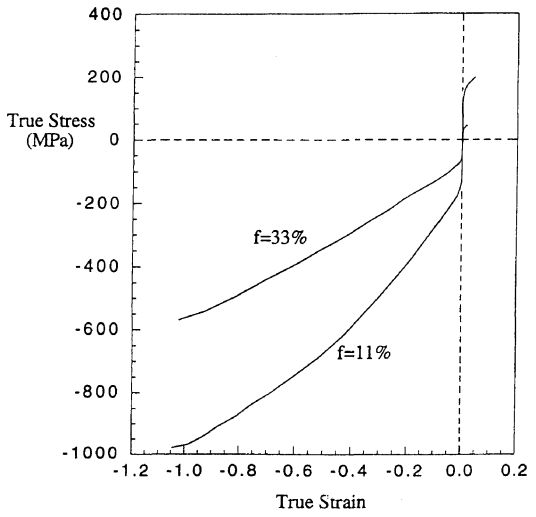

Fig. 1 Uniaxial true stress versus ture strain response for the sintered bronze, at $f=11\%$ and $f=33\%$

designed machining rig mounted in a screw driven test machine, as shown in Fig. 2 Cutting force F, transverse force T and tool displacement v were measured simultaneously.

Figure 3 shows typical variation of cutting pressure, i.e. F normalized by depth of cut d and thickness of specimen t plotted as against tool displacement v. During the continuous chip formation the cutting force asymptotes to a steady state with increasing tool displacement as indicated by the upper two lines in Fig. 3. But during a discontinuous chip formation the cutting force fluctuates with a constant wave length as indicated by the lowest line. Experimental results for the tool of the rake angle 45° are summarized in Table 2, where wave length $\lambda=0$ means the continuous chip formation. Optical and scanning

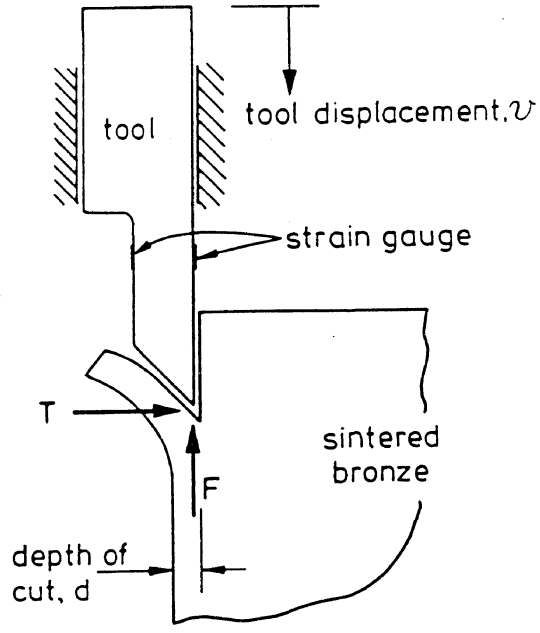

Fig. 2 Schematic diagram of machining rig and specimen

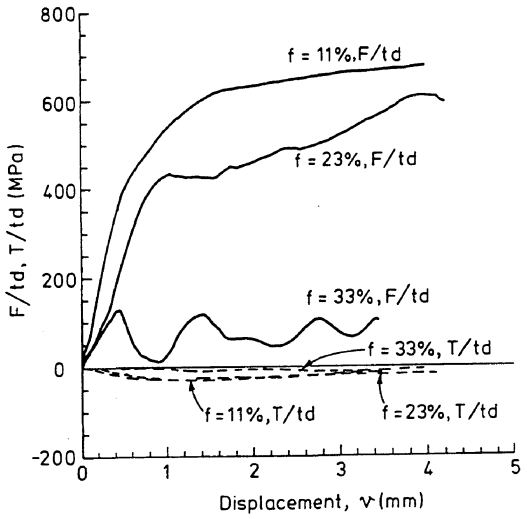

Fig. 3 Obseved normal cutting pressure F/td and transverse cutting pressure T/td plotted against tool displacement v, for a cutting depth of 0.4mm and porosities in the range of 11% to 33%

Table 2 Cutting test results

	$f=33\%$					$f=23\%$				$f=11\%$			
$d(mm)$	0.17	0.38	0.42	1.08	1.88	0.21	0.42	1.0	1.75	0.33	0.52	1.17	2.21
$\lambda(mm)$	0.45	1.0	1.0	2.2	3.0	0	0	4.0	5.0	0	0	5	8
$\frac{F_{max}}{td}$(MPa)	188	132	110	81	66	510	595	320	174	670	635	359	294

electro-microscopies for the cutting process showed that the continuous chip forms by compaction due to indentation of cutting edge followed by shear in a diffuse zone emanating from the tip of the tool. The discontinuous chip forms by repetition of compaction followed by fracture, i.e. crack growth from the tip of the tool towards the free surface of the chip. For details of the experiments and the results, see the reference (Fleck et al., 1996).

3. Theoretical Analysis

As mentioned above the cutting of the sintered bronze is composed of three processes, that is, compaction due to the indentation by cutting edge, the shear and the fracture near the chip root. Each process is analyzed using a model as follows.

3.1 Compaction due to indentation by the cutting edge

In early stage of machining the indentation by the cutting edge compacts the material, that is, the porosity local to the cutting edge is reduced. Fleck et al. (1992) showed that even for porous solids the indentation pressure using a Vickers pyramidal indenter is represented by

$$\frac{F}{A}=k\sigma_{yc} \tag{1}$$

where k is a constant given by the initial porosity and weakly dependent upon the indenter angle. A is the projected area of the indentation and σ_{yc} is the compressive yield stress. Figure 4 shows the schematic diagram for the indentation by the cutter tip. The projected area A for this machining is represented as

$$A=tv\tan(90^\circ-\alpha)$$

where t is the specimen thickness, v is the tool displacement and α is the tool rake angle. Therefore, from the Eq. (1), the cutting pressure due to the indentation is represented by

$$\frac{F}{td}=\frac{F}{A}\frac{A}{td}=k\sigma_{yc}\frac{\tan(90^\circ-\alpha)}{d}\cdot v \tag{2}$$

The cutting pressure F/td is proportional to v and inversely proportional to d.

3.2 Steady-state shear

After the compaction due to the indentation proceeds to a certain extent, some of the material slides over the rake face of tool to form chip while most of the plastic deformation, i.e. shear takes place in a diffuse zone emanating from the tip of the tool. We assume classical machining theory to be applicable. According to the theory (Oxley, 1989) the cutting and transverse pressure are given by

$$\frac{F}{td}=\tau_0\frac{\cos(\beta-\alpha)}{\sin\phi\cos(\phi+\beta-\alpha)}$$

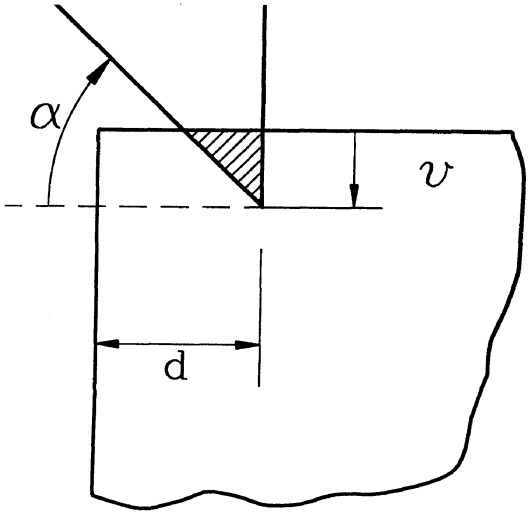

Fig. 4 Geometry of a specimen and the cutting tool during initial indentation

Table 3 Flow stresses and cutting pressure for steady state shearing

Porosity, f	σ_{yc}(MPa)	σ_0(MPa)	F/td(MPa)
33%	55	400	486
23%	95	500	608
11%	140	750	910

$$\frac{T}{td}=\tau_0\frac{-\sin(\beta-\alpha)}{\sin\phi\cos(\phi+\beta-\alpha)} \tag{3}$$

where the friction angle $\beta=\tan^{-1}\mu$, τ_0 is the shear flow stress and ϕ is the shear angle, which is typically given as (Oxley, 1989)

$$\phi=C_1-C_2(\beta-\alpha)$$

where $C_1=45°\pm10\sim15°$, $0.5\leq C_2\leq1$. We assume that ϕ is given as the mean, i.e.

$$\phi=45°-0.75(\beta-\alpha) \tag{4}$$

From the Eq. (3) the friction factor is represented by

$$\mu=\tan\beta=\frac{-\frac{T}{F}+\tan\alpha}{1+\frac{T}{F}\tan\alpha}$$

The results of this machining experiments showed that for the rake angle $\alpha=45°$

$$\frac{T}{F}\fallingdotseq-0.05$$

regardless of the porosity of the material or the existence of tool relief. Consequently the friction factor for $\alpha=45°$ is $\mu=1.105$, so that from the Eqs. (3) and (4)

$$\phi=42.853°$$
$$\frac{F}{td}=2.106\ \tau_0 \tag{5}$$

The shear flow stress τ_o is likely bigger than the initial yield stress because the material is significantly hardened, as shown in Fig. 1, during the initial compaction followed by shearing. The τ_o is estimated as follows; according to the classical machining theory, the shear strain γ during the continuous chip formation is given by

$$\gamma=\cos\phi+\tan(\phi-\alpha)$$

Substituting $\phi=42.853°$ and $\alpha=45°$ into this equation, the shear strain $\gamma=1.0404$ is obtained. Assuming Mises material and the state of pure shear, the equivalent stress σ_o is read from Fig. 1 corresponding to $\varepsilon_o=\frac{\gamma}{\sqrt{3}}=0.6010$. Then the shear flow stress τ_o is obtained from the relation $\tau_o=\frac{\sigma_o}{\sqrt{3}}$ for the state of pure shear. Substituting into the Eq. (5), the cutting pressure due to the steady-state shear is obtained. Table 3 shows the compressive yield stress σ_{yc}, the equivalent stress σ_o and the cutting pressure F/td for each porosity f.

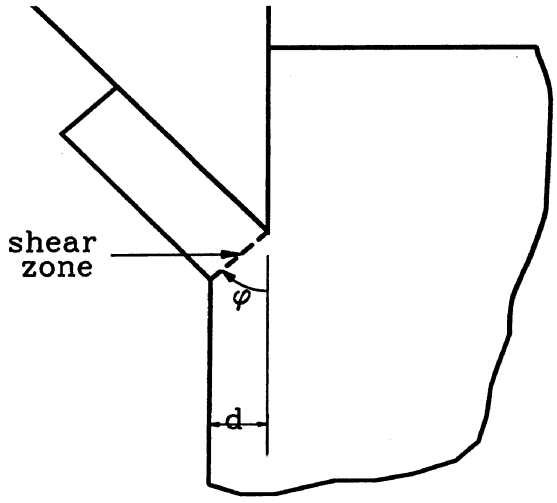

Fig. 5 Geometry of a specimen and the cutting tool during steady state shear

3.3 Fracture near the chip root

If the stress local to the tool is over a certain limit, a crack develops from the tip and grows towards the free surface of the chip. We assume elastic-brittle behavior. The geometry and loading is simulated by a subsurface short crack subject to uniform edge compression as shown in Fig. 6. According to Thouless et al. (1987) the stress

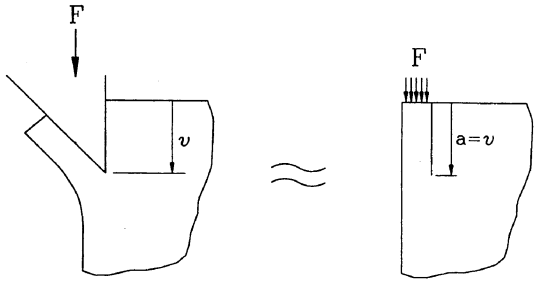

Fig. 6 Idealization of geometry/load of a specimen being machined by a tip of the cutting tool

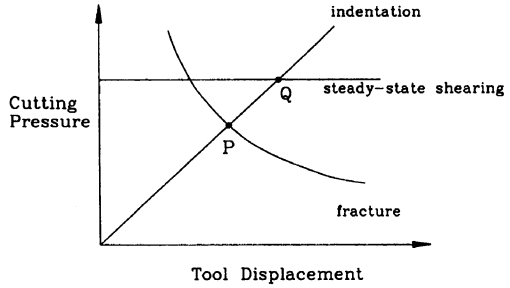

Fig. 7 Variation of cutting pressure against tool displacement due to the each process, i.e., indentation, fracture and steady state shear (dimension) (dimension)

intensity factor K_I is given by

$$K_I=0.36\frac{F}{td}\sqrt{a} \tag{6}$$

On identifying $K=K_{Ic}$ and crack length $a=v$, the cutting pressure the on the fracture is estimated to be

$$\frac{F}{dt}=\frac{K_{Ic}}{0.36\sqrt{v}} \tag{7}$$

4. Estimation of the Cutting Behavior

Figure 7 shows a schematic diagram of relations between the tool displacement and the cutting pressure for indentation, the steady-state shear and the fracture which are represented by the Eqs. (2), (5) and (7), respectively. At the point P in the figure the cutting pressure for the indentation is equal to the one for the fracture, while at the point Q the cutting pressure for the indentation is equal to the one for the steady-state shear. If the P is lower than the Q as shown in Fig. 7, the indentation is followed by the fracture, which results in the discontinuous chip formation. Otherwise, that is, if the P is higher than the Q, the shear occurs after the indentation, which results in the continuous chip formation.

Combining the Eqs. (2) and (7), the critical tool displacement v_c corresponding to the point Q is obtained as

$$v_c=\left(\frac{K_{Ic}}{0.36k\sigma_{yc}\tan(90^\circ-\alpha)}d\right)^{2/3} \tag{8}$$

where $\alpha=45^\circ$ and $k=3$ for fully dense metals and even porous metals of upto 30% porosity (Fleck et al., 1992). If the material and geometry are given, the critical tool displacement v_c is obtained as a function of the depth of cut d using the Eq. (8). Because the wave length of the cutting force λ is about 2 times v_c as shown in Fig. 3, the Eq. (8) gives estimation of the λ during the discontinuous chip formation. Figure 8 shows the plot of λ-d for the specimens of various porosities f. Here the symbols ○, △, □ represent the experimental results for $f=33\%$, 23%, 11%, respectively, and the lines represent the results estimated using the Eq. (8) The results with $\lambda=0$ mean the continuous chip formation, so the Eq. (8) is not applicable. In the case of discontinuous chip formation, i. e. $\lambda\neq0$, the estimated results agree well with the

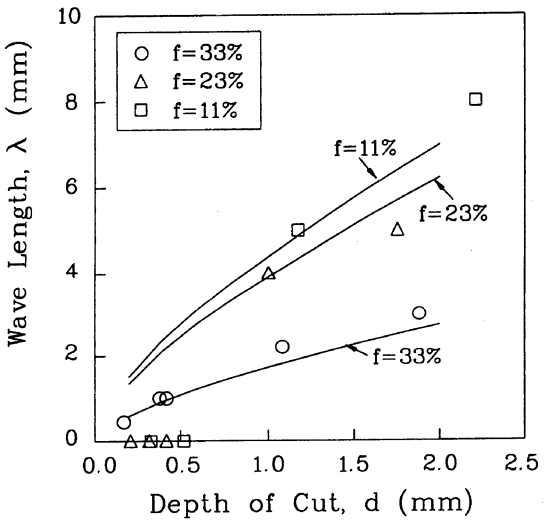

Fig. 8 Variation of wave length of chip formation against cutting depth for the specimens of various porosities f. Symbols ○, △, □ represent experimental results for $f=38\%$, 23%, 11%, respectively, and lines represent the results estimated using Eq. (8).

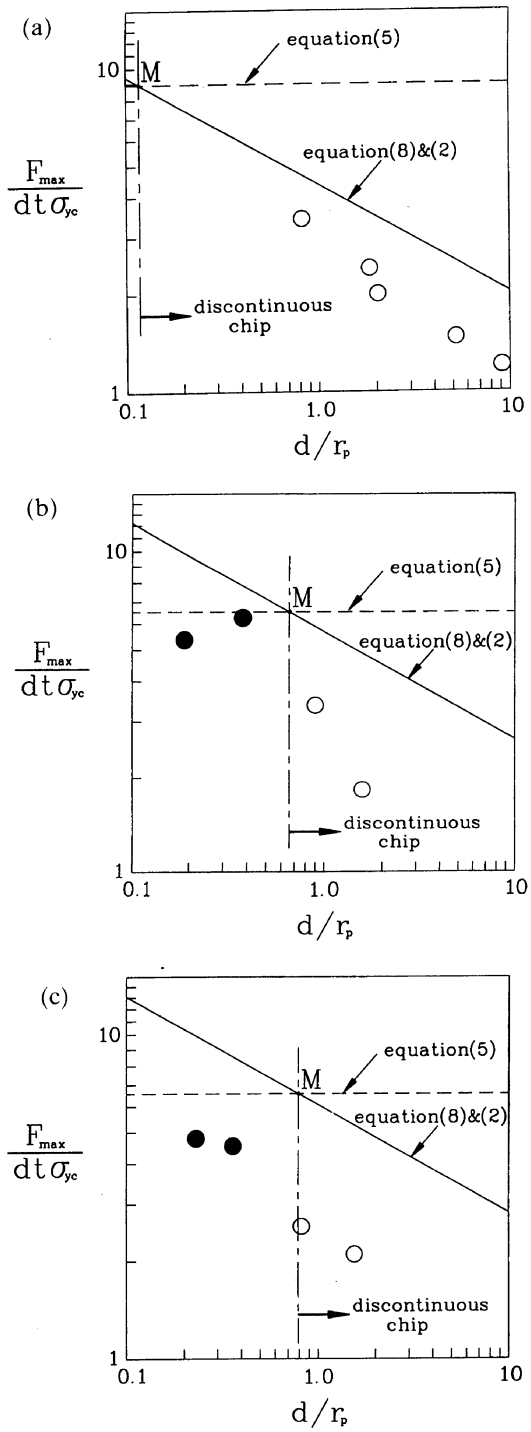

Fig. 9 Variation of non-dimensional cutting pressure against cutting depth normalized by the plastic zone size d/r_p for (a) $f=33\%$, (b) $f=23\%$, (c) $f=11\%$, respectively. Symbols ● and ○ represent experimental results during continuous and discontinuous chip formation, respectively. Solid lines represent the ones estimated from Eq. (2) with Eq. (8) while dashed lines represent the ones estimated from Eq. (5)

experimental ones considering the approximations involved.

Substituting the obtained v_c to the Eq. (2), the corresponding cutting pressure F_{max}/td is calculated. Figs. 9(a)~(c) show the non-dimensional plots of F_{max}/td versus d/r_p for $f=33\%$, $f=23\%$, $f=11\%$, respectively, where r_p is the plane strain plastic zone size at the onset of brittle fracture, i.e.

$$r_p=\frac{1}{3\pi}\left(\frac{K_{Ic}}{\sigma_{yt}}\right)^2$$

Here the solid and open circles represent the experimental results during the continuous and discontinuous chip formation, respectively. And the solid lines represent the ones estimated from the Eqs. (2) with (8) for the discontinuous chip, i. e. corresponding to the indentation-fracture system while the dashed lines represent the ones estimated from the Eq. (5) for the continuous chip, i.e. corresponding to the indentation-shear system. At the point M in Figs. 9 (a)~(c) the cutting pressure for the both systems is identical, so that M gives the critical depth of cut. If the depth of cut is bigger than the critical value corresponding to M, the cutting pressure for indentation-shear system is bigger than the one for indentation-fracture system, which results in the discontinuous chip formation. Otherwise, the continuous chip occurs. Predictions for the types of the chip formation on the basis of the point M agree well with the experimental results. Also the estimations of the cutting pressure versus depth of cut show reasonable agreement with the experiments considering the simplified models and approximation involved.

5. Concluding Remarks

The several behaviors observed during the machining of the sintered bronze can be explained. The lower the porosity f is, the lower K_{Ic} is, which gives the lower cutting pressure F/td via the Eq. (7). This promotes tendency of the discontinuous chip formation as shown in Fig. 7. Effect of the depth of the cut d can be interpreted via the Eq. (5) to (8). The F/td for the steady-state shear is independent of d while F/td for the

indentation-fracture system in inversely proportional to d, which is in favor of the discontinuous chip formation. Consequently the bigger depth of cut d likely yields the longer wave length λ and the lower F/td as shown in Figs. 8 and 9.

We think that this approach can be applied to the other materials, such as ceramics and rocks and that the parameters for machining, for example, the depth of cut can be pre-determined for given surface roughness, cutting force and porosity.

Effect of the tool rake angle has not been explored because of insufficient experimental results. More experiments are needed for it. For the rake angle $\alpha \approx 0$ or $\alpha < 0$, the indentation model described in this paper would not be valid because the compaction with the obtuse angled tool cannot be simulated by an indentation on semi-infinite media. For other processes, that is, for the shear and fracture, the presented models could be applied yet.

References

Fleck, N. A., Kang, K. J. and Williams, J. A., 1996, "The machining of Sinterd Bronze," *International Journal of Mechanical Science*, Vol. 38, No. 2, pp. 141~155.

Fleck, N. A., Otoyo, H. and Needleman, A., 1992, "Indentation of Porous Solids," *International Journal of Solids and Structures*, Vol. 29, No. 13, pp. 1613~1636.

Oxley, P. L. B., 1989, *The Mechanics of Machining, Ellis-Horwood, Chichester*.

Thouless, M. D., Evans, A. G., Ashby, M. F. and Hutchinson, J. W., 1987, "The Edge Cracking and Spalling of Brittle Plates," *Acta Metal*, Vol. 35, pp. 1333~1341.